Earthquakes and Structures, *Vol. 30, No. 3 (2026) 397-416*
https://doi.org/10.12989/eas.2026.30.3.397

Techno-Press

Empirical spectral amplification modeling for near-fault ground motions: Evidence and modification factors from the 2023 Kahramanmaraş earthquake sequence

Ömer Faruk Nemutlu[1], Mohamed Freeshah[2*]

[1]Civil Engineering Department, Faculty of Engineering and Architecture, Bingol University, Bingol, Türkiye
[2]Civil and Environmental Engineering Department, College of Engineering, United Arab Emirates University, Khalifa Bin Zayed St., Al Ain P.O. Box 15551, United Arab Emirates

(Received January 10, 2026, Revised February 18, 2026, Accepted February 23, 2026)

Abstract. Near-fault ground motions are often influenced by forward rupture directivity effects, which may generate distinctive long-period velocity pulses and substantially increase seismic demands compared to far-field records. However, conventional design spectra prescribed in seismic codes generally fail to incorporate these near-fault characteristics, potentially resulting in unconservative structural designs. This study examines the spectral amplification associated with near-fault effects and introduces a coefficient-based modification approach derived through regression analysis. A total of 20 ground motion records from the 6 February 2023 Mw 7.7 Pazarcık earthquake were employed - 10 near-fault and 10 far-field - and to account for the bidirectional nature of seismic excitation, both the East-West (EW) and North-South (NS) components were analyzed separately, yielding 40 datasets. Five-percent-damped elastic acceleration response spectra were computed using the Newmark-Beta method across a broad period range, after which average spectra for the near-fault and far-field groups were compared and spectral ratios were calculated to quantify amplification due to fault proximity. The period range was classified into short (T<0.5 s), medium (0.5 s≤T≤ 3 s), and long (T>3 s) intervals, and constant amplification coefficients were determined for each category. A regression-based model was further developed to represent the amplification trend as a function of period. An overall spectral modification factor of 1.47 was identified, and when applied to design spectra, this coefficient effectively reduced discrepancies between code-based and response spectra, mitigating potential underestimations. These findings emphasize the importance of explicitly incorporating near-fault effects in seismic design procedures.

Keywords: coefficient-based modification; near-fault ground motions; Pazarcik earthquake; seismic design; spectral amplification

1. Introduction

Seismic design codes around the world, including those adopted in regions of high seismicity, generally provide standardized acceleration response spectra intended to represent typical ground motions for a given hazard level. These spectra are typically derived from far-field records and assume relatively uniform energy distribution across frequencies and durations. However, in recent decades, the growing body of recorded near-fault ground motions especially from large-magnitude

*Corresponding author, Assistant Professor, E-mail: mfreeshah@uaeu.ac.ae

http://www.techno-press.org/eas/5 ISSN: 2092-7614 (Print), 2092-7622 (Online)

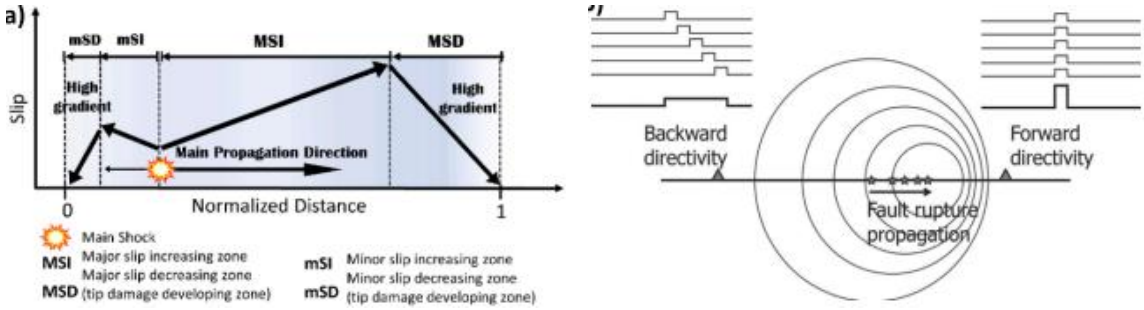

(a) (b)

Figure 1. Illustration of earthquake propagation and directivity effect [15, 16]

earthquakes has revealed that these records often deviate significantly from such assumptions. Near-fault earthquakes are characterized by unique features such as long-period velocity pulses, permanent ground displacements, and strong directionality effects due to rupture directivity [1-3]. These characteristics can lead to severe amplification of structural demands, particularly for medium-to-long-period structures, which are highly sensitive to pulse-type inputs [4].

Despite these well-documented effects, most seismic design codes still lack explicit modifications to address the increased demands from near-fault ground motions. This omission can result in unconservative estimates of structural response and potentially unsafe designs, especially for buildings, bridges, and lifelines situated close to active faults. The need to bridge this gap between recorded behavior and design assumptions serves as the main motivation for this study. By quantifying the amplification in spectral response caused by near-fault effects and comparing it to far-field motions, this research aims to derive practical amplification coefficients that can be applied to standard design spectra. Furthermore, the use of regression-based models enables a period-dependent spectral modification approach, making it more adaptable to performance-based seismic design practices.

Response spectra have long been fundamental tools in earthquake engineering, representing the peak response of single-degree-of-freedom (SDOF) systems subjected to seismic ground motions [5]. The concept was introduced in the early 20th century and has since evolved as a standard method for characterizing seismic demand on structures. Response spectra typically display spectral acceleration, velocity, or displacement as a function of vibration period, and are used extensively in seismic design codes worldwide [6-9]. The accuracy of response spectra is critical for reliable structural analysis, risk assessment, and design, as they condense complex time-history data into manageable engineering parameters. Classical methods for deriving response spectra often assume linear elastic behavior and uniform damping ratios, typically 5%, to standardize comparisons across different ground motions [10].

Near-fault ground motions differ significantly from far-field motions due to the proximity of the seismic source and the associated directivity effects. One of the most distinctive features of near-fault records is the presence of large velocity pulses often referred to as “forward directivity pulses” which result in long-period, high-amplitude ground velocity pulses (Shown in Fig. 1). The rupture directivity effects cause significant spatial changes in the ground motion amplitude and duration around the fault [4]. This effect creates significant differences between the horizontal ground motion components perpendicular and parallel to the fault direction. The study shows that these differences start especially at periods above 0.6 seconds and become more pronounced as the period increases [11]. These pulses can impose substantial demands on structures, especially those with natural periods close to the pulse period. The presence of pulse-like features can cause amplified structural responses that are not fully captured by traditional design spectra [12, 13]. Studies have demonstrated that ignoring near-fault effects can underestimate seismic demand, potentially leading to unsafe designs. Recent research emphasizes the need to account for pulse-like motions when developing seismic hazard assessments and designing structures in near-fault zones [14].

To address the limitations of conventional response spectra under near-fault conditions, various spectral modification approaches have been proposed. One common strategy involves scaling or adjusting spectral ordinates using amplification factors derived from empirical or simulation-based studies [17]. Some methods focus on augmenting design spectra by incorporating pulse effects through time-domain modifications or spectral shape adjustments [18]. Others employ statistical analyses on recorded near-fault motions to derive period-dependent modification coefficients or spectral modification factors [19]. Regression-based models have been increasingly used to generalize these modifications, enabling engineers to apply correction factors as functions of period and distance from the fault. Despite advances, challenges remain in developing universally applicable and robust modification schemes due to the complexity and variability of near-fault ground motions. Consequently, ongoing research continues to refine these approaches, aiming for improved accuracy and practical implementation in seismic design codes [20].

Near-fault effects lead to spectral amplifications in a narrow frequency band due to forward strike. Sgobba et al. [21] analyzed 230 pulse-like records in the NESS1 database to evaluate the role of these effects on spectral magnitudes. The pulse characteristics produced significant spectral deviations compared to the ordinary records; these differences were quantitatively modeled with the proposed amplification factors [21].

Long-period pulse components in near-fault records can transfer high amounts of energy to the structure in a short time and cause serious damage. This situation causes high displacement, and energy demands especially in the weak areas of the structure. In Mollaioli et al.'s study [22], the response of both linear and nonlinear single degree of freedom systems to this pulse effect was investigated with parameters derived directly from ground motion and energy-based spectral analyses. The findings revealed that near-fault records with forward directivity can carry structural demands, especially in terms of energy and displacement, well above the limits foreseen by the codes. In addition, equivalent pulse models that can represent these effects were defined [22].

High velocity pulses in near-fault ground motions cause structures located in these regions to become more susceptible to seismic damage. However, the limited number of available near-fault ground motion records necessitates the synthesis of such records in structural design. In this context, it is an important problem that traditional synthesis methods created by superimposing low and high frequency components in the time domain show large differences with the target spectrum. To overcome this problem, a new synthesis approach based on the spectral features of near-fault ground motions was developed by Zhang et al. [23] using a comprehensive database. In the developed method, the deficiencies of existing techniques were determined, and two separate correction strategies were proposed to ensure spectrum compatibility. The synthesized sample ground motions confirmed the suitability of the proposed method to the target spectrum [23].

The main objective of this study is to examine the effects of near-fault ground motions on elastic response spectra and to quantify the level of spectral amplification introduced by such effects through a coefficient-based modification approach. Ultimately, the study aims to propose a simplified, coefficient-based method for modifying standard design spectra to better account for near-fault effects, thereby contributing to improved accuracy in seismic design and performance evaluation of structures exposed to near-fault ground motions.

2. Data and method

The study specifically aims to highlight how the presence of velocity pulses and rupture directivity near fault zones influences spectral demands, particularly in comparison with typical far-field motions. To achieve this, ground motion records from the February 6, 2023, 7.7 M_w Pazarcık earthquake are classified into near-fault and far-field categories based on their proximity to the fault and their pulse-like characteristics. The elastic response spectra with 5% damping are calculated using the Newmark-Beta method for both the East-West and North-South components of each record. The spectral responses of the two record groups are then compared to identify systematic differences across various period ranges. By computing average spectra for both categories, the study investigates period-dependent amplification patterns and determines spectral modification coefficients by evaluating the ratio of near-fault to far-field spectra. These coefficients are further grouped according to defined period intervals ($T<0.5$ s, 0.5 s$<T<3$ s, and $T>3$ s) to represent short-, mid-, and long-period structural behaviors. A regression analysis is then conducted to express these ratios as continuous functions of period.

This study focuses on the evaluation of spectral amplification due to near-fault ground motions, particularly those generated by the February 6, 2023, M_w 7.7 Pazarcık earthquake. The scope is limited to analyzing elastic response spectra with a damping ratio of 5%, computed for both East-West and North-South components of 20 ground motion records (10 near-fault and 10 far-field), resulting in a total of 40 records. These records were selected from stations at varying distances from the fault to ensure a reliable comparison between near-fault and far-field conditions in literature and in this study, ground motion records were classified into near-fault and far-fault groups based on seismological characteristics, waveform features, and commonly adopted criteria in the literature. Near-fault records were selected from previous studies and databases focusing on motions recorded close to the fault rupture and exhibiting forward-directivity effects, typically characterized by distinct long-period velocity pulses. Far-fault records were defined as motions recorded at larger rupture distances, lacking pulse-like characteristics, and representing conventional spectral behavior. The adopted classification and record selection strategy are consistent with established approaches in near-fault ground motion research. [15, 24-27]. The analysis involves calculating the spectral response using the Newmark-Beta method [28], deriving average spectra for each record group, computing spectral amplification ratios, and establishing period-dependent modification factors. These coefficients are grouped and statistically evaluated within three predefined period intervals: short-period ($T<0.5$ s), mid-period (0.5 s$<T<3$ s), and long-period ($T>3$ s). A regression analysis is also performed to generalize the relationship between the period and amplification ratio. However, the study has certain limitations. First, only one earthquake event is considered, which may limit the generalizability of the results to other seismic regions or tectonic settings. Second, the analysis is confined to linear elastic behavior and does not account for inelastic structural response. Third, while the study uses both horizontal components, vertical ground motion effects are not included. Lastly, classification of records into near-fault and far-field categories is based on simplified criteria such as distance and pulse-like characteristics, which may involve some subjectivity. Despite these limitations, the study offers valuable insight into the quantitative effects of near-fault phenomena on spectral response and provides a

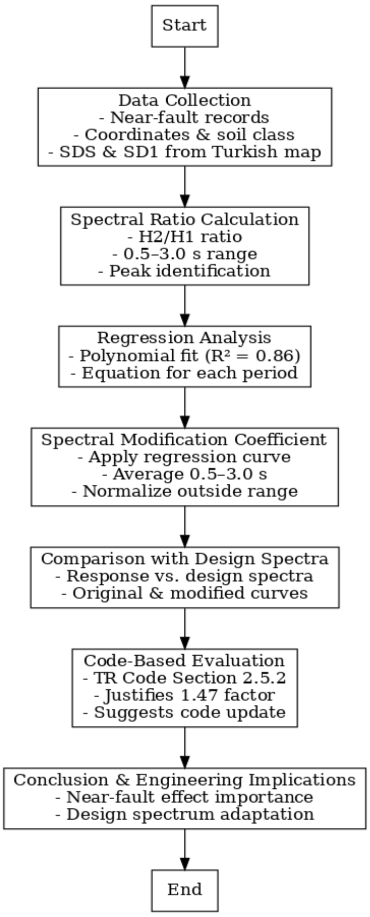

Figure 2. Schematic representation of the analysis workflow

coefficient-based framework that can be further refined and extended in future studies.

In this study, the classification of ground motion records into near-fault and far-fault groups was primarily based on R_{JB} distance and documented near-fault characteristics reported in previous studies. Near-fault records were selected from stations located within proximity to the causative fault and exhibiting strong directivity-related features commonly associated with near-fault ground motions. Formal pulse-detection algorithms, such as those proposed by Baker or Shahi and Baker, were not explicitly applied, as the primary objective of this study is not pulse characterization but the evaluation of code-based response spectra against observed near-fault spectral demands. This approach ensures consistency with practical seismic design frameworks, where near-fault effects are typically addressed through distance-based classification rather than algorithmic pulse identification. Distance was used as an initial screening parameter; however, the final classification also considered documented near-fault characteristics, particularly the presence of pulse-like features associated with rupture directivity. Near-source records do not necessarily induce extraordinary structural demand unless they contain pulse-type motions.

The overall procedure followed in this study has been summarized in a flow chart to enhance clarity and to provide a visual representation of the analysis steps. As illustrated in Fig. 2, the

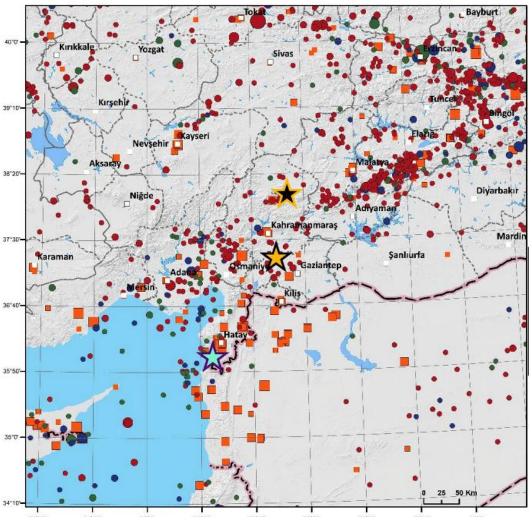

Figure 3. Map of epicenters for the Kahramanmaraş earthquakes and associated aftershocks [31]

(a)

(b) (c)

Figure 4. Progressive collapsed buildings example from Kahramanmaras Earthquakes [34]

process begins with the collection of near-fault ground motion data and the extraction of seismic parameters based on Turkish Seismic Hazard Map [29]. This is followed by the calculation of spectral ratios, identification of dominant peaks, regression analysis using a polynomial fit, and derivation of a spectral modification factor. Subsequently, response spectra of ground motions are compared with code-based design spectra, and implications for seismic code provisions are discussed. This step-by-step diagram enables a clear understanding of the analytical framework adopted in the study.

2.1 Kahramanmaraş earthquake sequences

On February 6, 2023, two very strong main earthquakes centered in Kahramanmaraş occurred in southeastern Türkiye. The first earthquake had a magnitude of 7.7 M_w and occurred on the Eastern Anatolian Fault System with the Ölüdeniz fault line and the epicenter in Pazarcık. This tremor caused severe ground movements in a wide area in the region. The length of the ruptured fault segment is approximately 300 km [30]. The second major earthquake was recorded on the same day, approximately 9 hours later, with a magnitude of 7.6 M_w and the epicenter in Elbistan on a neighboring fault segment, the Çardak fault zone, which is one of the branches of the Eastern Anatolian Fault Zone. The map displaying the epicenters of the Kahramanmaraş earthquakes and the aftershock activities is shown below in Fig. 3 [31]. 11 provinces in southeastern Türkiye were directly affected by the earthquake. 14 million people living in these 11 cities were affected by the earthquake [32], and over 50000 people lost their lives. Around 250000 structures were completely unusable, collapsed or severely damaged (Fig. 4). In the field observations made after the earthquake, the cities most affected by the earthquake were Malatya, Hatay, Kahramanmaras and Adiyaman [33]. There are many studies in the literature evaluating the structural damage and earthquake characteristics in these cities [34-37]. Both earthquakes released a great deal of energy and created high acceleration and long-term ground motions, especially in areas affected by near-faults. The earthquakes occurred with consecutive ruptures in multiple fault segments, which caused the ground movements to exhibit a complex structure. Due to the forward directivity effect, sudden, high-amplitude and long-period pulse-like waves were observed in the ground motions [13]. These characteristics were decisive in the extraordinary levels of earthquake-induced damage and structural demands [3]. In addition, extensive aftershocks and many fault ruptures of different sizes were observed in the Kahramanmaraş earthquake region [34]. This earthquake sequence has once again revealed the tectonic activity and earthquake hazard in a region that is critically important in terms of earthquake activity and fault lines in Türkiye.

2.2 Selection and classification of ground motion records

The Kahramanmaraş earthquake sequence impacted 11 provinces in southeastern Türkiye: Adana, Adıyaman, Diyarbakır, Elazığ, Gaziantep, Hatay, Kahramanmaraş, Kilis, Malatya, Osmaniye, and Şanlıurfa. The affected region spans approximately 110,000 km^2 and was home to more than 13.5 million people before the earthquakes (1). Fig. 1 presents the geographic distribution of the 304,299 analyzed buildings across the earthquake-affected region. The map visualization uses optimized coordinate bounds (36-40°E longitude, 36.5-39°N latitude) to focus specifically on the building distribution area, eliminating empty geographical regions. The spatial concentration patterns clearly reflect urban development density and proximity to the fault rupture zones of the February 6, 2023, earthquake sequence.

Table 1. Key characteristics of the selected ground motion records

	Station	Latitude	Longitude	R_{JB} (km)	NS (cm/s^2)	EW (cm/s^2)
Near-fault records	3123	36,21423	36,15973	72,58341	655,57128	593,9403986
	3124	36,2387	36,1722	69,66107	572,63231	638,3214265
	3125	36,23808	36,13264	70,81593	822,61604	1121,947964
	3126	36,2202	36,1375	72,55381	1178,1156	999,383067
	3129	36,19117	36,1343	75,70543	1351,5002	1198,743469
	3139	36,58383	36,41439	28,54152	577,13066	504,8208471
	4614	37,48513	37,29775	8,254134	2165,5843	2175,076596
	4615	37,38676	37,13803	8,018127	582,31369	583,7049721
	2708	37,09933	36,64837	2,587456	1294,82	1294,82
	2718	37,00777	36,6266	2,095246	654,43082	630,3120444
Far-fault records	0201	37,76121	38,26742	48,06106	478,07148	911,3041564
	3146	36,49076	36,22695	41,57225	483,84558	346,9314602
	4404	38,19588	38,87385	117,7143	136,24371	137,416246
	4405	38,8107	37,9396	125,5608	91,118286	126,4966785
	4612	38,02395	36,48187	95,79456	140,97002	122,2219667
	4626	37,57532	36,91505	35,49416	108,80812	223,0931427
	6303	37,7524	39,3291	117,3498	117,42257	114,439434
	6304	37,36509	38,51316	55,38302	210,89718	238,2281967
	8003	37,08417	36,26936	27,11038	141,56686	185,7379028
	8004	37,37989	36,09763	61,05423	168,42611	181,8594248

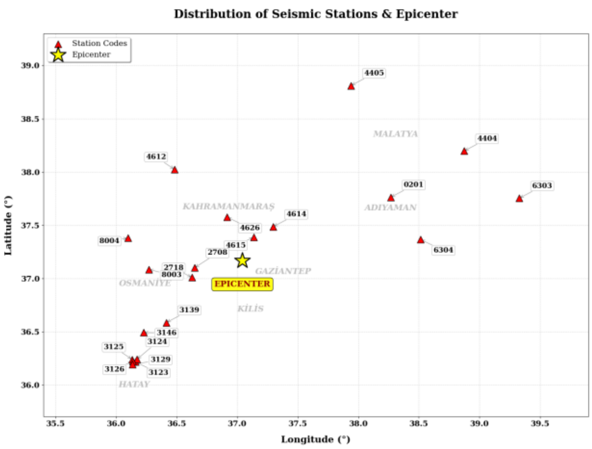

Figure 5. Location map of near-fault and normal ground motion records considered in this study

The earthquake records used in this study are classified into two groups as "with near-fault effect" and "without near fault effect". This distinction allows for more accurate analysis of ground motion characteristics and structural behavior in earthquake engineering and structural assessment studies. Since the near-fault effect significantly affects the characteristics and magnitude of ground motions recorded during earthquakes, the necessity of taking this effect into consideration is frequently emphasized in the literature. The earthquake records used in the study were selected from reliable sources in the current literature and obtained from the TADAS (Turkish Accelerometric Database and Analysis System) database [38]. TADAS is a platform that includes different earthquake parameters and provides a wide data set for research. In this context, the selected records were evaluated in both East-West (EW) and North-South (NS) directions to expand the scope of the analysis and increase the reliability of the results. Within the scope of the study, a total of 40 individual earthquake records belonging to the February 6 Kahramanmaraş earthquake were analyzed. The number and diversity of the selected records were determined to increase the statistical validity of the analyses and to ensure that the obtained results are compatible with the literature [15, 24, 26, 27]. The selection of earthquake records is an important stage that directly affects the accuracy of the analyses conducted and the validity of the findings obtained. The information regarding the earthquake records is presented in Table 1. Fig. 5 presents the locations of the selected ground motion stations used in this study. In this study, the distance parameter adopted for record classification is the Joyner-Boore distance (R_{JB}), defined as the shortest horizontal distance from the recording station to the surface projection of the rupture plane. The R_{JB} values reported in Table 1 were obtained directly from the official metadata provided by the Disaster and Emergency Management Authority (DEMA) ground motion database [38].

2.3 Response spectrum calculations

The response spectra utilized in this study were obtained using the SeismoSignal software [39]. In this process, the earthquake records specified in Section 2.2 were employed as input data for the software. For each individual earthquake record, response spectra corresponding to two distinct directions East-West and North-South were calculated separately. This methodology enables a comprehensive analysis of the seismic response characteristics for different orientations, thereby facilitating a more detailed examination of the ground motion effects on structural systems.

3. Methodology of spectral analysis

In this study, to determine the spectrum modification coefficient, earthquake records were divided into two groups according to the prominence of fault-induced effects: records with near-fault effects and records with distant-fault effects. Elastic ground motion response spectra with a damping ratio of 5% were calculated separately for both groups. The obtained spectra were evaluated in the period range from 0.05 seconds to 4 seconds and presented graphically for comparative analysis. In Fig. 6, the response spectra calculated for both groups of records are shown together, and the differences in spectral behaviors are visually demonstrated.
All analyses were performed on the acceleration records of the Kahramanmaraş-Pazarcik (M_w 7.7) earthquake that occurred on February 6, 2023. Both the east-west (EW) and north-south (NS) components of the records obtained from a total of 20 different stations were evaluated separately, thus the total number of spectra used in the analysis reached 40. Thanks to this systematic approach, the amplification levels of near-fault effects on spectral magnitudes were clearly observed and data were obtained that would form the basis for how these effects should be reflected in the design spectra.

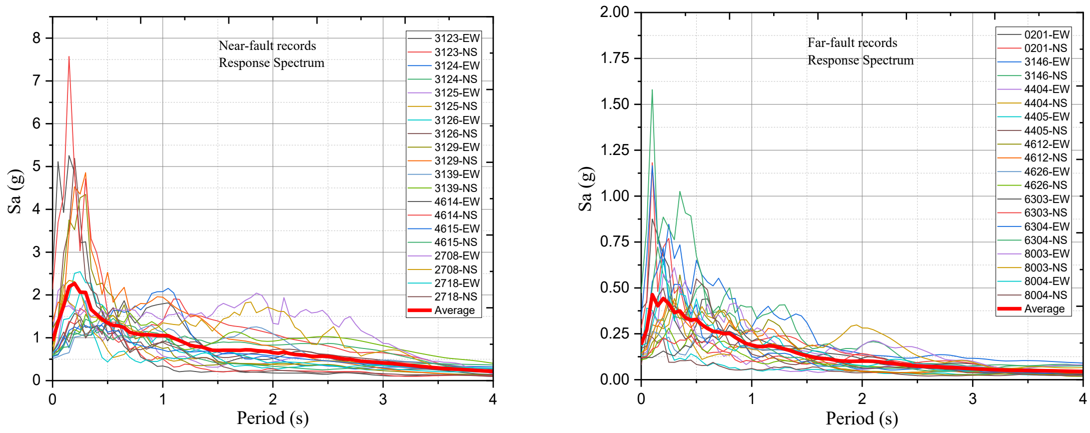

(a) Near-fault ground motion records (b) Far-fault ground motion records

Figure 6. Response spectra of the selected ground motion records

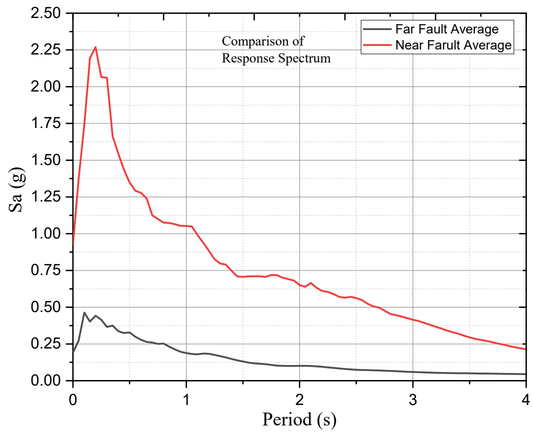

Figure 7. Comparison of average response spectra for near-fault and far-fault records

Using the response spectra derived from these 40 ground motion records, separate average spectra were computed for each group namely, near-fault and far-fault motions. The primary objective of obtaining average spectra was to quantify the variation observed across specific period ranges and to derive a representative ratio that captures this difference. In doing so, it becomes possible to characterize the amplification effect induced by near-fault conditions and to express its impact on design spectra in a quantitative manner.

Fig. 7 presents a comparative illustration of the average response spectra for both groups. As clearly seen in the figure, the average spectral accelerations of the near-fault group are significantly higher than those of the far-fault group across a wide range of periods, particularly beyond 0.6 seconds. This observation highlights the pronounced amplification caused by near-fault effects, which is often underestimated in conventional design spectra.

4. Spectral ratio and modification factor derivation

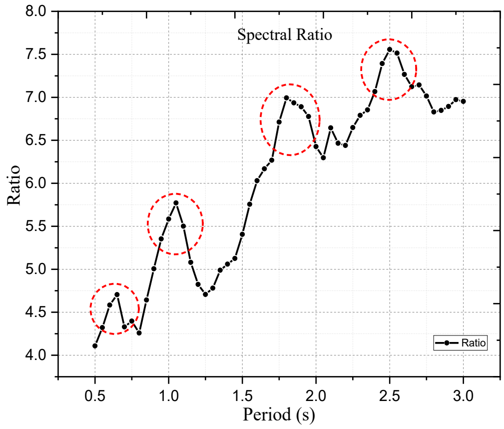

Figure 8. Spectral ratio peaks in the range of 0.5-3.0 seconds

In Fig. 7, the average response spectra corresponding to both near-fault and far-fault ground motion records were compared by evaluating their spectral ratio across the period range. The analysis revealed that the ratio between the two average spectra exhibited noticeable peaks particularly within the 0.5 to 3.0-second period interval. These local amplifications suggest that near-fault ground motions impose a distinct influence on the spectral shape, especially in the intermediate-period range. The presence of such peaks can be attributed to the directivity effects and long-period pulse-like characteristics typically associated with near-fault events.

While Fig. 7 presents the comparison between the average response spectra of near-fault and far-fault records, the period range exhibiting the most pronounced amplification differences is more clearly identified in the spectral ratio curves shown in Fig. 8. As observed in Fig. 8, the amplification effect becomes significantly more pronounced within the 0.5-3.0 s period interval, where near-fault records consistently exceed far-fault records. This observation supports the emphasis on the medium-to-long period range in the subsequent analyses.

Further illustration of these peaks is provided in Fig. 8, where the spectral ratio curve is presented in detail for the 0.5-3.0 s period range. The peak points, representing the most significant amplifications, are highlighted with red circles to facilitate visual interpretation. This graphical representation reinforces the critical need to account for near-fault amplification in the development or adjustment of design spectra.

4.1 Regression analysis for coefficient modeling

Following the identification of peak points, a regression analysis was conducted based on the spectral ratio curve. As an initial step, the data were discretized to isolate key amplification points. Subsequently, the most suitable functional form to represent the observed behavior of the spectral ratio peaks was investigated. Among the tested models, the polynomial function was found to provide the best fit for the empirical data. Upon selecting the polynomial regression model, the curve was fitted accordingly, and the model was calibrated to derive the corresponding polynomial coefficients. The R^2 for the polynomial regression was calculated as 0.86, indicating a strong correlation between the model and the observed data. The resulting regression equation, along with the fitted polynomial curve and the original spectral ratio profile, is presented in Fig. 9. This

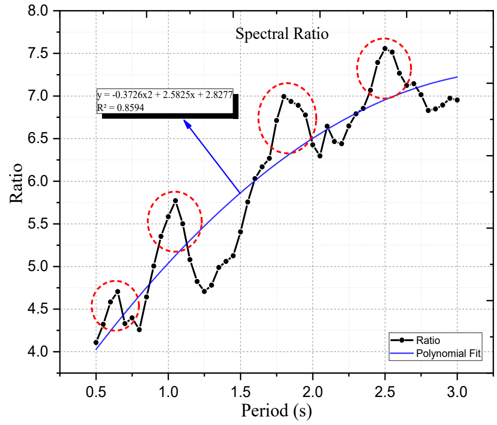

Figure 9. Regression analysis for the spectral ratio modification

Table 2. Period-dependent application of regression coefficients for spectral modification

Period	Equation	Period	Equation	Period	Equation	Period	Equation	Period	Equation	Period	Equation
0	2,8277	0,5	4,0258	1	5,0376	1,5	5,8631	2	6,5023	2,5	6,9552
0,05	2,9559	0,55	4,1354	1,05	5,1285	1,55	5,9354	2,05	6,5560	2,55	6,9902
0,1	3,0822	0,6	4,2431	1,1	5,2176	1,6	6,0058	2,1	6,6078	2,6	7,0234
0,15	3,2067	0,65	4,3489	1,15	5,3048	1,65	6,0744	2,15	6,6577	2,65	7,0547
0,2	3,3293	0,7	4,4529	1,2	5,3902	1,7	6,1411	2,2	6,7058	2,7	7,0842
0,25	3,4500	0,75	4,5550	1,25	5,4736	1,75	6,2060	2,25	6,7520	2,75	7,1118
0,3	3,5689	0,8	4,6552	1,3	5,5553	1,8	6,2690	2,3	6,7964	2,8	7,1375
0,35	3,6859	0,85	4,7536	1,35	5,6350	1,85	6,3301	2,35	6,8389	2,85	7,1614
0,4	3,8011	0,9	4,8501	1,4	5,7129	1,9	6,3894	2,4	6,8795	2,9	7,1834
0,45	3,9144	0,95	4,9448	1,45	5,7889	1,95	6,4468	2,45	6,9183	2,95	7,2035
0,5	4,0258	1	5,0376	1,5	5,8631	2	6,5023	2,5	6,9552	3	7,2218
Mean	3,4407	Mean	4,5457	Mean	5,4643	Mean	6,1967	Mean	6,7427	Mean	7,1025
Unit	1	Ampl.	1,321139	Ampl.	1,588132	Ampl.	1,80098	Ampl.	1,959682	Ampl.	2,064239

Table 3. Coefficients to be used in the amplification procedure for specific period intervals

0-0,5	0,5-1	1-1,5	1,5-2	2-2,5	2,5-3	3-3,5	3,5-4	Mean
1	1,32	1,59	1,8	1,96	2,06	1	1	1,47

functional representation offers a practical means of incorporating near-fault amplification effects into spectral modification procedures.

Although slight amplification is observed in the 0-0.5 s period range (Table 2), the magnitude of this increase is relatively limited compared to the medium-to-long period interval. Since the most pronounced and structurally significant amplification occurs between 0.5-3.0 s, the regression analysis and coefficient derivation presented in Table 3 primarily focus on this range. Nevertheless, for practical design implementation, the final amplification factor was applied to the entire response spectrum, as illustrated in Fig. 10, to maintain simplicity and usability within a

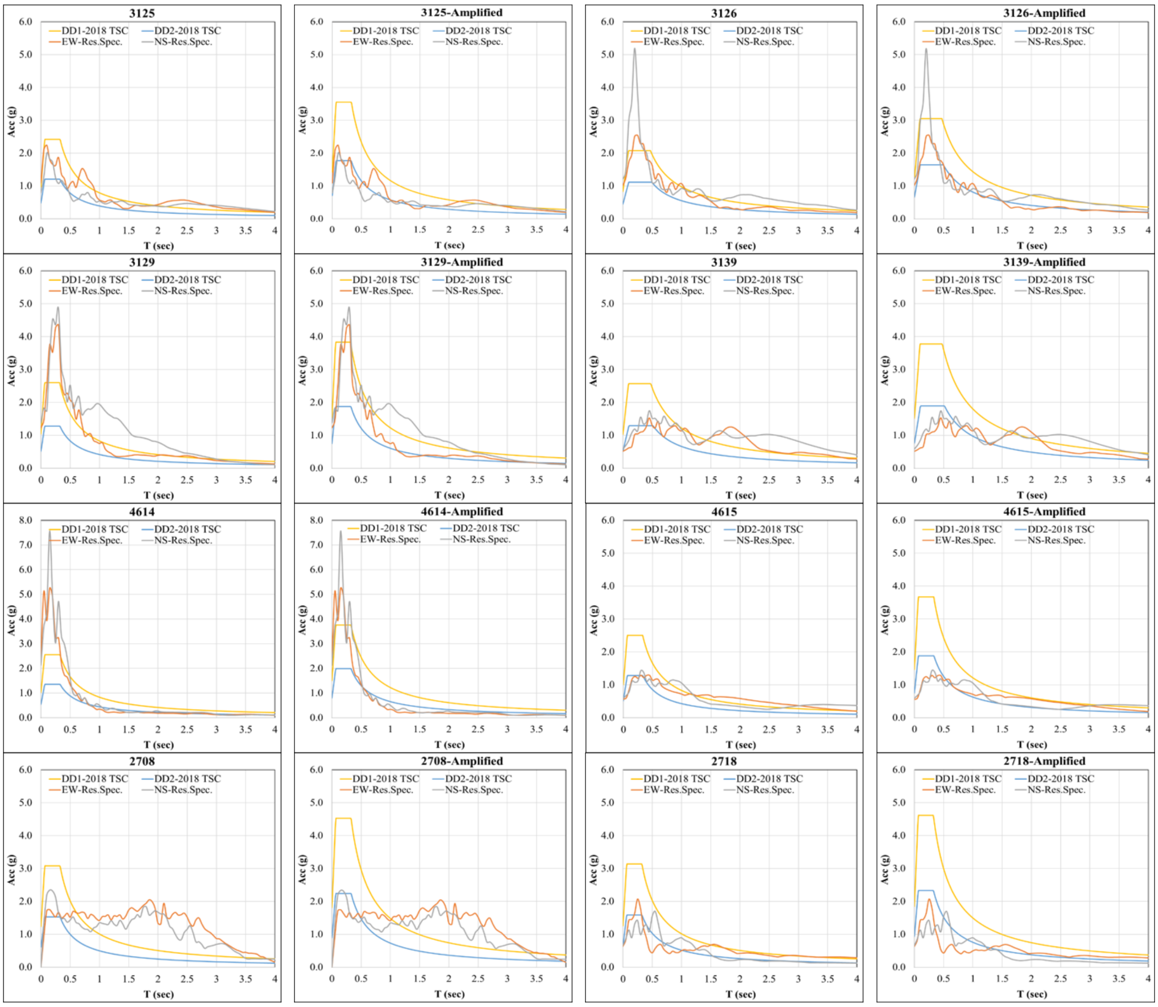

Figure 10. Comparison of amplified and unamplified response spectra with TBDY-2018 design spectra

code-oriented framework.

Subsequently, the regression equation derived from the analysis was applied to each period value within the 0.5 s to 3.0 s range. The resulting values for each period are presented in the "equation" column of Table 2. The amplification factor reported as "Ampl." in Table 2 was obtained by applying the regression equation to each period within the 0.5-3.0 s interval and computing the arithmetic mean of the resulting values. This average value represents a single equivalent spectral modification coefficient for the specified period range. To obtain a representative amplification factor for this period range, the average of these values was calculated. For periods outside the 0.5 to 3.0 second interval, an amplification factor of unity was assumed. This approach enabled the determination of the amplification coefficients used to modify the spectral ordinates accordingly.

Table 3 presents the variation of the amplification coefficients obtained for each period range. Since these coefficients are intended to be applied to existing design spectra, a single representative amplification factor is required. Therefore, the average of the coefficients calculated for the different period intervals was taken to derive a unified value for spectral amplification. As shown in Table 3, the resulting amplification factor determined in this study is 1.47. Although a single representative amplification factor is proposed, its application is limited to the 0.5-3.0 s period range, where near-fault spectral amplification is dominant. Outside this interval, no additional amplification is recommended. Therefore, the proposed modification should be interpreted as a period-dependent, piecewise spectral adjustment rather than a uniform scaling of the entire response spectrum.

5. Discussion

The influence of near-fault ground motions on structural response has long been a critical subject in earthquake engineering, particularly due to the presence of forward-directivity and fling-step effects that result in large velocity pulses. These distinct features significantly alter the spectral content of ground motions, especially within the intermediate period range, leading to increased seismic demands on structures located in proximity to fault lines. Despite the well-documented impact of such ground motions, current seismic design codes often fail to explicitly address the amplification effects observed in the response spectra of near-fault records. In this context, a more comprehensive understanding of spectral amplifications caused by near-fault effects is essential for developing reliable design spectra and ensuring structural safety under these demanding conditions. The findings of this study carry important implications for both structural design practices and seismic code development, particularly in regions with potential near-fault seismic hazards. The observed spectral amplifications, especially within the intermediate period range, indicate that current design spectra may underestimate seismic demand in such scenarios. Incorporating the proposed amplification factors into design procedures could lead to more accurate seismic assessments and improve the resilience of structures against near-fault ground motions. Furthermore, the proposed methodology has potential applications in developing site-specific design spectra, updating hazard maps, and calibrating fragility functions for performance-based earthquake engineering. These applications highlight the need for refined modeling approaches that can capture the unique characteristics of near-fault ground motions in both deterministic and probabilistic frameworks.

As part of the analytical framework, S_{DS} and S_{D1} values corresponding to the coordinates and site classifications of ten near-fault stations listed in Table 4 were extracted from the official Turkey Earthquake Hazard Map. These parameters were obtained for both DD1 and DD2 seismic design levels, in accordance with the Turkish Building Earthquake Code 2018 (TBDY 2018) [8]. The primary motivation for retrieving these code-based spectral parameters was to enable a comparative assessment of the recorded ground motions against standard design spectra. This approach provides a basis for evaluating how well current code spectra reflect the actual demands imposed by near-fault ground motions and facilitates the identification of potential underestimations in spectral ordinates within critical period ranges.

Following the acquisition of code-based seismic parameters, the design spectra defined by the TBDY 2018 were plotted alongside the response spectra derived from the recorded ground motions. These comparative visualizations are presented in Fig. 10 through two separate graphs. The first graph illustrates the comparison between the standard design spectra and the empirical response spectra, whereas the second graph compares the amplified design spectra adjusted based

Table 4. TBDY-2018 based data of the stations where ground motion records were obtained (for Near-fault records)

Information about records included near fault effect								DD1		DD2	
Station	Latitude	Longitude	R_{JB}	PGA (cm/s^2)	PGA (g)	Vs_{30} (m/s) *	Soil Class*	S_{DS}**	S_{D1}**	S_{DS}**	S_{D1}**
3123	36,21423	36,15973	72,58	655,57	0,668267	470	ZC	2,532	0,819	1,253	0,408
3124	36,2387	36,1722	69,66	638,32	0,650683	283	ZD	2,066	0,978	1,12	0,555
3125	36,23808	36,13264	70,82	1121,95	1,14368	448	ZC	2,417	0,791	1,205	0,391
3126	36,2202	36,1375	72,55	1178,12	1,200938	350	ZD	2,076	0,977	1,119	0,553
3129	36,19117	36,1343	75,71	1351,5	1,377676	447	ZC	2,606	0,833	1,277	0,414
3139	36,58383	36,41439	28,54	577,13	0,588308	272	ZD	2,57	1,224	1,29	0,663
4614	37,48513	37,29775	8,25	2178,72	2,220917	541	ZC	2,557	0,833	1,352	0,442
4615	37,38676	37,13803	8,02	584,65	0,595973	484	ZC	2,501	0,827	1,284	0,428
2708	37,09933	36,64837	2,58	1294,82	1,319898	523	ZC	3,08	1,007	1,526	0,5
2718	37,00777	36,6266	2,74	592,35	0,603823	572	ZC	3,143	1,019	1,588	0,517

*: The Vs30 values were obtained from station recordings. The soil classes were determined according to the Vs30 values based on TBDY-2018 Table 16.1.

**: The S_{DS} and S_{D1} spectral coefficients were taken from the tdth.afad.gov.tr site based on coordinates [40].

on the proposed modification factor with the same response spectra. This dual-graph approach aims to highlight the inadequacy of unmodified code spectra in capturing the spectral demands induced by near-fault ground motions and to demonstrate the improvement achieved through spectral amplification.

When the design spectra amplified by the factor of 1.47 are examined, a significant improvement in spectral compatibility is observed. In the case of a major seismic event such as the Kahramanmaraş earthquakes, this amplification proves particularly effective for the DD1 ground motion level, where the amplified spectra align more closely with the expected design performance. Notably, the spectra modified using the 1.47 factor effectively mitigate the excessive spectral demands observed beyond the 0.5-second period—typically attributed to near-fault effects—by keeping the design spectra within acceptable bounds. This outcome underscores the importance of introducing a spectral modification factor to ensure safety and compliance in near-fault seismic design scenarios.

Previous studies have proposed period-dependent or pulse-based near-fault modification models, primarily focusing on capturing the physical characteristics of velocity pulses and forward directivity effects. In contrast, the objective of this study is not to introduce a new pulse-based formulation, but to evaluate the adequacy of code-based design spectra in representing near-fault spectral demands using observed ground motion data. The proposed amplification factor of 1.47 is derived by focusing on the medium-to-long period range (0.5-3.0 s), where near-fault effects are most pronounced and structurally critical. Unlike period-dependent functions, the use of a single averaged factor provides a practical and directly applicable adjustment within current design frameworks, particularly for regions governed by the TBDY-2018. This approach prioritizes engineering applicability and consistency with design practice rather than detailed pulse characterization.

According to Section 2.5.2 of the TBDY-2018 (Scaling of Earthquake Records Using the

Simple Scaling Method), the resultant horizontal spectrum is defined as the square root of the sum of the squares of the two horizontal components of each selected ground motion record [41-44]. The average of these resultant spectra, calculated for all selected records, must satisfy the condition that the amplitude ratio between the average spectrum and the design spectrum—defined according to Sections 2.3.4 or 2.4.1—within the period range of 0.2 T to 1.5 T, should not be less than 1.3. Furthermore, both horizontal components are required to be scaled using the same scaling factor [8].

Considering this provision, the spectral amplification factor of 1.47 obtained in this study is not only consistent with the current code requirements but also suggests that the prescribed lower limit of 1.3 might be subject to reevaluation. The results point to the potential need for updating the existing code provisions, particularly in regions where near-fault effects significantly alter ground motion characteristics. International seismic codes address near-fault effects through different strategies. ASCE 7 introduces near-fault factors applied to spectral ordinates, while Eurocode 8 indirectly accounts for such effects through spectral shape and record selection criteria [6, 7]. Japanese design practice emphasizes site-specific record selection and scaling. Compared to these approaches, the proposed factor in this study offers a simplified, data-driven adjustment calibrated directly against observed near-fault ground motions from a major Turkish earthquake sequence, providing a region-specific and code-compatible alternative.

Although period-dependent amplification factors provide a more detailed representation of spectral modification, the present study adopts a single averaged amplification coefficient for practical engineering implementation. The primary objective is to propose a simplified, design-oriented adjustment that can be readily incorporated into existing code-based response spectra. While a period-dependent formulation may capture spectral characteristics more explicitly, the use of a single coefficient enhances usability and facilitates straightforward application within the current regulatory framework. The development of period-dependent amplification models tailored to Turkish near-fault conditions may constitute a valuable direction for future research.

Several previous studies have incorporated near-fault effects within the framework of Ground Motion Prediction Equations (GMPEs) by introducing distance-dependent or pulse-related modifiers. For example, Chang et al. [45] proposed an empirical narrowband model to account for amplification effects induced by near-fault directivity. Unlike GMPE-based approaches, which aim to predict ground motion intensity measures for hazard assessment, the present study focuses on the modification of design response spectra based on observed spectral amplification patterns. Therefore, the proposed amplification factor is intended as a practical design-oriented adjustment rather than a predictive GMPE formulation.

In this study, distance was primarily used as a classification parameter to distinguish near-fault and far-fault records. A more systematic incorporation of distance as a continuous variable within the amplification model may further improve accuracy. This aspect is recommended for future research.

Although the present study is based on a single earthquake sequence, the use of multiple stations and bidirectional components provides a sufficiently robust dataset to investigate near-fault spectral amplification under a consistent seismotectonic setting.

It should be noted that the proposed spectral amplification factor is derived without explicit differentiation between site categories. While site effects are already incorporated by S_{DS} and S_{D1} values in the TBDY-2018, future studies may further refine the amplification model by stratifying records according to soil classes and investigating site-dependent near-fault effects.

Although the present study does not explicitly decompose pulse-like characteristics or directional components of individual ground motion records, the observed spectral amplifications in the medium-to-long period range (0.5-3.0 s) are consistent with the well-documented effects of forward directivity and velocity pulses reported in the literature [11, 15, 27]. Previous studies have demonstrated that pulse-like motions and directionality primarily amplify spectral ordinates at longer periods, which is in line with the trends identified in this study through spectral ratio analyses. The primary objective of this research is not to isolate pulse mechanisms at the record level, but rather to evaluate the adequacy of code-based design spectra in capturing near-fault-induced spectral demands. A detailed component-wise or azimuth-dependent investigation may be considered as a subject of future research.

6. Conclusions

The results obtained in this research clearly indicate that the standard design spectra are often insufficient in capturing the increased demands posed by near-fault ground motions, leading to possible underestimations in structural performance assessments. The comparative analyses carried out in this study, based on both ordinary and near-fault records from the February 6, 2023, Pazarcık (M_w 7.7) earthquake, demonstrate that the amplification coefficient of 1.3 recommended by the Turkish Building Earthquake Code 2018 (TBDY-2018) is inadequate in fully capturing the increased spectral demands induced by near-fault conditions. To address this gap, a modification coefficient of 1.47 is proposed based on the comparative analysis of response spectra derived from near-fault and ordinary ground motion records. The application of this amplification factor to the design spectra has shown to mitigate the exceedance issue in several cases, aligning the spectral demands more accurately with those observed under real near-fault scenarios. When applied to design spectra, this coefficient effectively mitigates the issue of spectral exceedance observed in near-fault records, particularly at periods exceeding 0.6 seconds, where rupture directivity effects become significant. Although the findings are based on a limited data set consisting of 20 records (40 components) from February 6, 2023, Pazarcik earthquake this approach provides a robust foundation for spectral modification strategies. Future studies can enhance the reliability of the proposed coefficient by incorporating a larger set of ground motion records from multiple seismic events, and by categorizing the motions based on site conditions. Such advancements would enable a more specialized understanding of spectral behavior and lead to refined, site-specific modification models for seismic design under near-fault conditions.

This study emphasizes the significant influence of near-fault ground motions on the seismic response of structures, particularly due to their distinct spectral characteristics and pulse-like behavior. Despite their potential to amplify seismic demands, current seismic design codes do not explicitly incorporate near-fault effects into the definition of design spectra such as Turkish Building Earthquake Code (TBDY 2018).

- Near-fault effects are currently not adequately considered in existing earthquake design codes, leading to potential underestimation of seismic demands on structures.
- This study demonstrates that design spectra require an amplification factor to account for near-fault ground motion characteristics and proposes a coefficient of 1.47 for this purpose.
- Application of the 1.47 amplification factor to spectral ordinates reduces or eliminates the problem of spectral demand exceedance observed in some cases when near-fault effects are present.
- Comparative analyses based on the TBDY-2018 reveal that the existing amplification factor

of 1.3 is insufficient to capture the true impact of near-fault motions.

• The methodology and findings presented here can be extended to include multiple earthquake scenarios and different site conditions, improving the spatial specificity of spectral modifications.

• Future studies incorporating a larger set of ground motion records and soil classification are recommended to further refine amplification factors and enhance their applicability in seismic design [46-48].

Acknowledgements

This research was funded by the UAE University grant number 12N264. The authors acknowledge the Turkish Seismic Hazard Map for near-fault ground motion data and the extraction of seismic parameters. We also express our gratitude to Turkish Accelerometric Database and Analysis System (TADAS) for the earthquake records.

References

1. Champion, C., Liel, A. (2012). The effect of near-fault directivity on building seismic collapse risk. Earthquake Engineering & Structural Dynamics, 41, 1391-1409. https://doi.org/10.1002/eqe.1188.
2. Alavi, B., Krawinkler, H. (2004). Behavior of moment-resisting frame structures subjected to near-fault ground motions. Earthquake Engineering & Structural Dynamics, 33, 687-706. https://doi.org/10.1002/eqe.369.
3. Bray, J.D., Rodriguez-Marek, A. (2004). Characterization of forward-directivity ground motions in the near-fault region. Soil Dynamics and Earthquake Engineering, 24, 815-828. https://doi.org/10.1016/j.soildyn.2004.05.001.
4. Somerville, P.G. (2003). Magnitude scaling of the near fault rupture directivity pulse. Physics of the Earth and Planetary Interiors, 137, 201-212. https://doi.org/10.1016/S0031-9201(03)00015-3.
5. Chandramohan, R., Baker, J.W., Deierlein, G.G. (2016). Quantifying the influence of ground motion duration on structural collapse capacity using spectrally equivalent records. Earthquake Spectra, 32, 927-950. https://doi.org/10.1193/122813eqs298mr2.
6. American Society of Civil Engineers (2017). Minimum design loads and associated criteria for buildings and other structures (ASCE 7-16). American Society of Civil Engineers, Reston, VA, USA.
7. European Committee for Standardization (2005). Eurocode 8: Design of structures for earthquake resistance (EN 1998). European Committee for Standardization, Brussels, Belgium.
8. AFAD (2018). Türkiye bina deprem yönetmeliği-2018 (TBDY-2018). Disaster and Emergency Management Authority (AFAD), Çankaya, Ankara, Türkiye.
9. Chopra, A.K. (2007). Dynamics of structures. Pearson Education, London, UK.
10. Bayraktar, A., Türker, T., Altunişik, A.C. (2015). Experimental frequencies and damping ratios for historical masonry arch bridges. Construction and Building Materials, 75, 234-241. https://doi.org/10.1016/j.conbuildmat.2014.10.044.
11. Somerville, P.G., Smith, N.F., Graves, R.W., Abrahamson, N.A. (1997). Modification of empirical strong ground motion attenuation relations to include the amplitude and duration effects of rupture directivity. Seismological Research Letters, 68, 199-222. https://doi.org/10.1785/gssrl.68.1.199.
12. Kramer, S.L. (1996). Geotechnical earthquake engineering. Prentice Hall, Englewood Cliffs, NJ, USA.
13. Tothong, P., Cornell, C.A., Baker, J.W. (2007). Explicit directivity-pulse inclusion in probabilistic seismic hazard analysis. Earthquake Spectra, 23, 867-891. https://doi.org/10.1193/1.2790487.
14. Adanur, S., Altunişik, A.C., Bayraktar, A., Akköse, M. (2012). Comparison of near-fault and far-fault

ground motion effects on geometrically nonlinear earthquake behavior of suspension bridges. Natural Hazards, 64, 593-614. https://doi.org/10.1007/s11069-012-0259-5.
15. Kazaz, İ., Bilge, İ.H., Gürbüz, M. (2024). Near-fault ground motion characteristics and its effects on a collapsed reinforced concrete structure in Hatay during the February 6, 2023 Mw7.8 Kahramanmaraş earthquake. Engineering Structures, 298, 117067. https://doi.org/10.1016/j.engstruct.2023.117067.
16. Singh, J.P. (1985). Earthquake ground motions: Implications for designing structures and reconciling structural damage. Earthquake Spectra, 1, 239-270. https://doi.org/10.1193/1.1585264.
17. Boore, D.M., Atkinson, G.M. (2008). Ground-motion prediction equations for the average horizontal component of PGA, PGV, and 5%-damped PSA at spectral periods between 0.01 s and 10.0 s. Earthquake Spectra, 24, 99-138. https://doi.org/10.1193/1.2830434.
18. Abrahamson, N.A., Silva, W.J. (1997). Empirical response spectral attenuation relations for shallow crustal earthquakes. Seismological Research Letters, 68, 94-109. https://doi.org/10.1785/gssrl.68.1.94.
19. Sheikh, M.N., Tsang, H.H., Yaghmaei-Sabegh, S., Anbazhagan, P. (2013). Evaluation of damping modification factors for seismic response spectra. Proceedings of the Australian earthquake engineering society conference 2013, Hobart, Tasmania, Australia, November.
20. Deoda, V.R., Adhikary, S. (2020). A preliminary proposal towards the revision of Indian seismic code considering site classification scheme, amplification factors and response spectra. Bulletin of Earthquake Engineering, 18, 2843-2889. https://doi.org/10.1007/s10518-020-00806-2.
21. Sgobba, S., Lanzano, G., Pacor, F., Felicetta, C. (2021). An empirical model to account for spectral amplification of pulse-like ground motion records. Geosciences, 11(1), 15. https://doi.org/10.3390/geosciences11010015.
22. Mollaioli, F., Bruno, S., Decanini, L.D., Panza, G.F. (2006). Characterization of the dynamic response of structures to damaging pulse-type near-fault ground motions. Meccanica, 41, 23-46. https://doi.org/10.1007/s11012-005-7965-y.
23. Zhang, C., Wu, C. Wang, P., Li, D., Lu, J. (2024). Improved methods for synthesizing near-fault ground motions based on specific response spectrum. Soil Dynamics and Earthquake Engineering, 183, 108790. https://doi.org/10.1016/j.soildyn.2024.108790.
24. Abdelmeguid, M. Zhao, C., Yalcinkaya, E., Gazetas, G., Elbanna, A., Rosakis, A. (2023). Dynamics of episodic supershear in the 2023 M7.8 Kahramanmaraş/Pazarcik earthquake, revealed by near-field records and computational modeling. Commun Earth Environ, 4, 456. https://doi.org/10.1038/s43247-023-01131-7.
25. Akinci, A., Dindar, A.A., Bal, I.E., Ertuncay, D., Smyrou, E., Cheloni, D. (2025). Characteristics of strong ground motions and structural damage patterns from the February 6th, 2023 Kahramanmaraş earthquakes, Türkiye. Natural Hazards, 121, 1209-1239. https://doi.org/10.1007/s11069-024-06856-y.
26. Chang, Z., Wu, H., Li, W., Yan, Z., Peng, L., Zhu, G. (2025). Analysis of near-fault ground motions in the February 2023 Kahramanmaras, Türkiye, earthquake sequence. Bulletin of Earthquake Engineering, 23(4), 1349-1369. https://doi.org/10.1007/s10518-025-02101-4.
27. Towhata, I., Çağlayan, P.Ö., Tönük, G., Erginağ, U.C., Sendir Torisu, S. (2025). Reconnaissance and Discussion on Ground Motion Induced by the 2023 Türkiye-Syria Earthquake. Journal of Earthquake Engineering, 29, 981-1022. https://doi.org/10.1080/13632469.2025.2458600.
28. Newmark, N.M., Hall, W.J. (1982). Earthquake spectra and design, vol. 3, engineering monographs on earthquake criteria, structural design, and strong motion records. Earthquake Engineering Research Institute, Berkeley, CA, USA.
29. Akkar, S., Azak, T., Can, T. O. L. G. A., Çeken, U., Demircioğlu Tümsa, M. B., Duman, T. Y., ... & Zülfikar, Ö. (2018). Evolution of seismic hazard maps in Turkey. Bulletin of Earthquake Engineering, 16, 3197-3228. https://doi.org/10.1007/s10518-018-0349-1.
30. Hussain, E., Kalaycıoğlu, S., Milliner, C.W.D., Çakir, Z. (2023). Preconditioning the 2023 Kahramanmaraş (Türkiye) earthquake disaster. Nature Reviews Earth & Environment, 4, 287-289. https://doi.org/10.1038/s43017-023-00411-2.
31. AFAD (2023). 06 Şubat 2023 Pazarcık-Elibstan Kahramanmaraş (Mw:7.7-Mw:7.6) Depremleri Raporu. Disaster and Emergency Management Authority (AFAD), Çankaya, Ankara, Türkiye.

32. Nemutlu, Ö.F., Sari, A., Balun, B. (2023). 06 Şubat 2023 Kahramanmaraş depremlerinde (Mw 7.7-Mw 7.6) meydana gelen gerçek can kayıpları ve yapısal hasar değerlerinin tahmin edilen değerler ile karşılaştırılması. Afyon Kocatepe University Journal of Sciences and Engineering, 23(5), 1222-1234. https://doi.org/10.35414/akufemubid.1302254.
33. Nemutlu, Ö.F. (2025). Loss analyses associated with the secondary effect in earthquake: A case study of Kahramanmaras earthquake sequences. Earthquakes and Structures, 28(2), 137-147. https://doi.org/10.12989/eas.2025.28.2.137.
34. Altunsu, E., Güneş, O., Öztürk, S., Sorosh, S., Sarı, A., Beeson, S.T. (2024). Investigating the structural damage in Hatay province after Kahramanmaraş-Türkiye earthquake sequences. Engineering Failure Analysis, 157, 107857. https://doi.org/10.1016/j.engfailanal.2023.107857.
35. Altunişik, A. C., Arslan, M. E., Kahya, V., Aslan, B., Sezdirmez, T., Dok, G., ..., Nas, M. (2023). Field observations and damage evaluation in reinforced concrete buildings after the February 6th, 2023, Kahramanmaraş-Türkiye earthquakes. Journal of Earthquake and Tsunami, 17(6), 2350024. https://doi.org/10.1142/S1793431123500240.
36. Akar, F., Işık, E., Avcil, F., Büyüksaraç, A., Arkan, E., İzol, R. (2024). Geotechnical and structural damages caused by the 2023 Kahramanmaraş earthquakes in Gölbaşı (Adıyaman). Applied Sciences, 14, 2165. https://doi.org/10.3390/app14052165.
37. Avcil, F., Işık, E., İzol, R., Büyüksaraç, A., Arkan, E., Arslan, M.H., Aksoylu, C., Eyisüren, O., Harirchian, E. (2024). Effects of the February 6, 2023, Kahramanmaraş earthquake on structures in Kahramanmaraş city. Nat Hazards, 120, 2953-2991. https://doi.org/10.1007/s11069-023-06314-1.
38. AFAD (2023). Turkish accelerometric database and analysis system (TADAS). Disaster and Emergency Management Authority (AFAD), Çankaya, Ankara, Türkiye. https://tadas.afad.gov.tr/
39. SeismoSoft (2021). SeismoSignal: Signal processing of strong motion data (Version 2021). SeismoSoft, Pavia, Italy. https://www.seismosoft.com/
40. Afet ve Acil Durum Yönetimi Başkanlığı (AFAD) (2025). Official website. Disaster and Emergency Management Authority (AFAD), Çankaya, Ankara, Türkiye. https://www.afad.gov.tr/
41. Nemutlu, Ö.F., Özçelik, S.T.A., Freeshah, M. (2025). A machine learning framework for regional damage assessment using multi-station seismic parameters: Insights from the 2023 Kahramanmaraş earthquakes. Buildings, 15(18), 3326. https://doi.org/10.3390/buildings15183326.
42. Uyanik, H., Kokum, M., Senturk, E., Freeshah, M., Ozcelik, S.T., Akpinar, M.H., ... Sengur, A. (2025). Seismic foresight: A novel multi-input 1D convolutional mixer model for earthquake prediction using ionospheric signals. IEEE Access, 13, 116200-116210. https://doi.org/10.1109/ACCESS.2025.3583749.
43. Saqib, M., Şentürk, E., Arqim Adil, M., Freeshah, M. (2024). Seismo-ionospheric precursory detection using hybrid Bayesian-LSTM network model with uncertainty-boundaries and anomaly-intensity. Advances in Space Research, 74(4), 1828-1842. https://doi.org/10.1016/j.asr.2024.05.023.
44. Uyanık, H., Şentürk, E., Akpınar, M.H., Ozcelik, S.T.A., Kokum, M., Freeshah, M., Sengur, A. (2023). A multi-input convolutional neural networks model for earthquake precursor detection based on ionospheric total electron content. Remote Sensing, 15(24), 5690. https://doi.org/10.3390/rs15245690.
45. Chang, Z., Sun, X., Zhai, C., Zhao J.X., Xie, L. (2018). An empirical approach of accounting for the amplification effects induced by the near-fault directivity. Bulletin of Earthquake Engineering, 16, 1871-1885. https://doi.org/10.1007/s10518-017-0275-7.
46. Thanh, P.T., Freeshah, M., Osama, N., Chien, L.H., Thom, T.T., Elshewy, M.A. (2025). Soil erosion risk and mitigation strategies in steep and complex forest ecosystems. Civil Engineering Journal, 11(8), 3358-3374. https://doi.org/10.28991/CEJ-2025-011-08-015.
47. Freeshah, M., Şentürk, E., Zhang, X., Livaoğlu, H., Ren, X., Osama, N. (2024). Investigating multiple ionospheric disturbances associated with the 2020 August 4 Beirut explosion by geodetic and seismological data. Pure and Applied Geophysics, 181, 875-894. https://doi.org/10.1007/s00024-023-03386-9.
48. Uyanik, H., Şentürk, E., Akpınar, M. H., Ozcelik, S.T.A., Kokum, M., Freeshah, M., Sengur, A. (2025). Seismic foresight: A novel multi-input 1D convolutional mixer model for earthquake prediction using ionospheric signals. IEEE Access, 13, 116200-116210. https://doi.org/10.1109/ACCESS.2025.3583749.